

Interactions among Cloud, Water Vapor, Radiation, and Large-Scale Circulation in the Tropical Climate. Part II: Sensitivity to Spatial Gradients of Sea Surface Temperature

KRISTIN LARSON AND DENNIS L. HARTMANN

Department of Atmospheric Sciences, University of Washington, Seattle, Washington

(Manuscript received 7 August 2002, in final form 11 November 2002)

ABSTRACT

The responses of the large-scale circulation, clouds, and water vapor to an imposed sea surface temperature (SST) gradient are investigated. Simulations compare reasonably to averaged observations over the Pacific, considering the simplifications applied to the model. The model responses to sinusoidal SST patterns have distinct circulations in the upper and lower troposphere. The upper circulation is sensitive to the heating from deep convection over the warmest SST. Stronger SST gradients are associated with stronger longwave cooling above stratus clouds in the subsidence region, stronger lower-tropospheric large-scale circulation, a reduction of the rain area, and larger area coverage of low clouds. A similar SST gradient with a warmer mean temperature produces slightly weaker lower-tropospheric circulation, and slightly reduced low cloud coverage.

The outgoing longwave radiation (OLR) is not sensitive to the mean SST or the range of the imposed sinusoidal SST gradient. The positive feedbacks of water vapor and decreasing high cloud OLR compensate for the increase in longwave emission with increasing mean temperature in these simulations. As the SST gradient is increased keeping the mean SST constant, the positive high cloud feedback is still active, but the air temperature increases in proportion to the maximum SST in the domain, increasing the clear-sky OLR value and keeping the average OLR constant.

The net absorbed shortwave radiation (SWI) is found to be extremely sensitive to the SST gradient. The stronger lower-tropospheric large-scale circulation produces a higher water content in the high and low clouds, increasing the absolute magnitude of the shortwave cloud forcing. A 25% increase in the maximum zonal mass flux of the lower circulation of the 300-K mean, 4-K SST range simulation leads to a 7.4 W m^{-2} decrease in SWI. Increasing the mean SST creates a positive feedback in these simulations because of the decrease in the lower-tropospheric large-scale circulation and the resultant decrease in cloud optical depth.

1. Introduction

Convection, clouds, and water vapor have the potential to produce large positive or negative feedbacks in the climate system. Feedbacks associated with the dependence of saturation vapor pressure on temperature are strongest in the Tropics, where the surface temperature is already high. These feedback processes are coupled in important ways to the large-scale circulation, which is, in turn, influenced by the spatial gradients of sea surface temperature (SST) and the distribution of land and sea.

Several different feedback processes are potentially important in the Tropics. The dependence of saturation vapor pressure on temperature gives a naturally strong positive feedback (Manabe and Wetherald 1967), which should be particularly strong in the Tropics. This feedback is altered by lapse rate feedback, because the moist-adiabatic lapse rate decreases significantly with tem-

perature (e.g., Cess 1975; Knutson and Manabe 1995). The greatest flux of infrared energy in the Tropics comes from dry, cloudless regions (Pierrehumbert 1995). If the area of the dry cloudless regions changes with temperature, or the relative humidity changes with temperature, then strong feedbacks might be associated with such changes (Lindzen 1990a; Lindzen et al. 2001, but see also Betts 1990; Lindzen 1990b; Hartmann and Michelsen 2002a,b; Lindzen et al. 2002).

If the albedo of tropical convective clouds is very sensitive to SST, then this can produce a strong negative feedback (Ramanathan and Collins 1991). Within the Tropics, however, convective cloud albedo is affected both by the absolute value of SST and the gradients of SST (Hartmann and Michelsen 1993). Lau et al. (1994) showed that the convective intensity and associated convective cloud albedo in a cloud-resolving model were much more sensitive to the imposed mean vertical motion than to the SST. In nature, the mean vertical motion appears to be modulated by the horizontal gradients of SST. In addition, stratocumulus clouds in the Tropics are particularly sensitive to SST gradients and may provide an important climate feedback (Miller 1997; Larson

Corresponding author address: Dr. Kristin Larson, Department of Atmospheric Sciences, University of Washington, Box 351640, Seattle, WA 98195-1640.
E-mail: klarson@atmos.washington.edu

et al. 1999). Coupled atmosphere–ocean models indicate that the simulated SST gradients are sensitive to cloud processes (Meehl et al. 2000), so that the cloud properties are determined by mutual interaction between the SST distribution, convection and clouds, and the large-scale circulation. Climate feedback processes may respond differently to changes in mean SST and changes in the gradients of SST in the Tropics. In this study, we will examine the relative roles of mean SST and SST gradients by studying a set of model experiments with imposed SST distributions with sinusoidal variations.

The effect of imposed SST gradients on tropical convection and clouds has been studied in a variety of atmospheric models. A 2D cumulus ensemble model (CEM) study by Grabowski et al. (2000) used an imposed sinusoidal SST gradient and studied the effects of cloud–radiative interaction. Bretherton and Sobel (2002) use quasi-equilibrium theory and the weak temperature gradient approximations to show similar sensitivities to cloud–radiation interaction as Grabowski et al. (2000). Both studies found the addition of cloud–radiation interaction reduces the fraction of the domain where it is raining and covered with deep convection. Bretherton and Sobel (2002) make the further prediction that the rain area will decrease with increasing SST gradient and the mean atmospheric temperature will increase with increasing SST gradient. Sui et al. (2000, manuscript submitted to *J. Climate*, hereafter SLLC) study a 2D CEM with a cold pool and a warm pool. The SST difference between the pools is varied and the precipitation increases with increasing SST difference and the precipitation area decreases. The radiative cooling and the subsidence strength remain constant, but the convective area decreases with increasing SST difference in their model. The net change of shortwave radiation is negligible and the outgoing longwave radiation (OLR) change is due to the water vapor greenhouse effect and the larger longwave effect of cloud forcing (SLLC).

Larson and Hartmann (2003, hereafter LH1) showed in Part I of this study that numerical experiments with uniform SSTs had increased high cloud with increasing SST, though the relative humidity profile showed only a weak dependence on SST. The insensitivity of the relative humidity profile to SST was also found in the numerical experiments of Tompkins and Craig (1999). LH1 also showed the sensitivity of the radiative fluxes to SST is similar to the sensitivity inferred from observations.

In Part II of this study, the model of LH1 is forced by sinusoidal SST gradients. The resulting large-scale circulations and their effects on the clouds, water vapor, and top of the atmosphere (TOA) radiation balances are discussed. Unlike most previous models, the model of LH1 has a realistic boundary layer cloud scheme, and this will prove to be important. Section 2 describes the model and compares it to observations. Section 3 investigates the large-scale circulation. Subsequently, the

precipitation, integrated water variables, clouds, radiation and their sensitivity to mean SST, and SST gradients of the model are investigated (sections 4, 5, and 6). Conclusions and discussion are in section 7.

2. Model description and validation

The essential physical processes of dynamics, cloud microphysics, convection, radiation, and moisture advection are included in the fifth-generation Pennsylvania State University–National Center for Atmospheric Research (PSU/NCAR) Mesoscale Model (MM5) version 2. The MM5 has been modified as in LH1. The Community Climate Model version 3 radiation code has been implemented as well as the shallow cumulus and boundary layer parameterizations based on Grenier and Bretherton (2001), McCaa (2001), McCaa et al. (2002, manuscript submitted to *Mon. Wea. Rev.*, hereafter MBG), and McCaa and Bretherton (2002, manuscript submitted to *Mon. Wea. Rev.*). The horizontal grid spacing is set to 120 km and the domain is 16 grid points by 160 grid points. The SST is prescribed to vary in the 160 grid-point direction, but it is constant across the 16 grid-point width. The simulations are computed for 90 days and the results reported are from averages of data every 6 h for days 60–90 of the simulation. The data are averaged over the shorter horizontal dimension of the simulations as well, since the SST does not change in that direction.

Equatorial Pacific observations are chosen to validate the model. The Pacific is the largest expanse of equatorial ocean on the planet and normally features a strong east–west temperature gradient along the equator. The model, with equatorial equinox insolation including the diurnal but no annual cycle, is compared to climatologies over the Pacific for the month of September. The average insolation for September is close to the equinox value, and that month has a large SST gradient over the Pacific, producing a strong Walker Circulation.

For comparison with observations, a sinusoidal SST gradient is chosen that approximates the SST distribution in the Equatorial Pacific for September. The SST data are from the Comprehensive Ocean–Atmosphere Data Set (COADS) climatology (version 1a for years 1980–95) and are averaged from 5°N to 5°S for 130°–230°E and smoothed; the average for September and the annual average are both shown (Fig. 1). The doubly periodic model spans a full sine wave, but only part of the domain is compared to observations because the SST distribution of the Pacific does not approximate a full period of a sine function. The range of SSTs used in the model is 3.9°C and the mean is 27.5°C. A narrow range of latitudes (5°N–5°S) is used for comparison to the model, since the SST does not vary with latitude in the model.

Tropospheric tropical temperatures do not have large horizontal temperature gradients above the boundary layer in the Tropics. Vertical profiles of temperature for

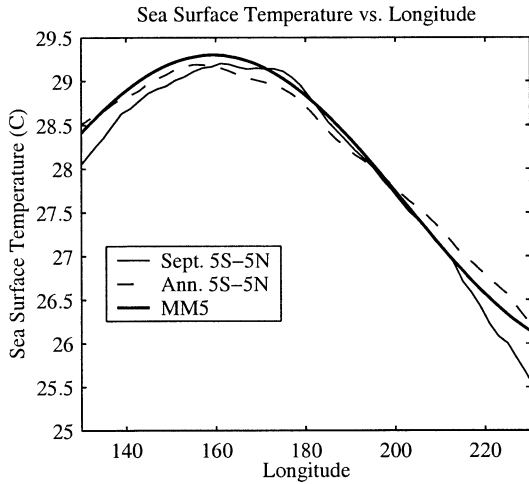


FIG. 1. SST vs longitude. The SSTs are from the COADS dataset. The annual averages (dashed) and the Sep monthly (solid thin) climatology are shown for latitudes averaged over 5°N–5°S. The model SST is denoted with a thick line.

the warmest (5°N–5°S, 150°–170°E) and coldest (5°N–5°S, 240°–260°E) parts of the model and the corresponding regions over the Pacific are shown (Fig. 2). Reanalysis datasets incorporate observations and previous results of numerical weather prediction. The National Centers for Environmental Prediction (NCEP) re-

analysis climatology is averaged for the years 1979–95 and the European Centre for Medium-Range Weather Forecasts (ECMWF) reanalysis is averaged for years 1980–89. NCEP and ECMWF reanalysis air temperatures are similar in both regions; the model temperature is cooler in the warm region and the upper troposphere of the cold region. The cold bias of this simulation is similar to the cold bias in the troposphere found in many cloud models when simulating convection over the western Pacific cold pool (Su et al. 1999). Mixing of very dry air from the troposphere to the planetary boundary layer may contribute to a deeper surface boundary layer with colder air temperatures in the warm pool (MBG). GCMs are also known to have a cold bias in the tropical upper troposphere. The cold bias in the CCM3 is 3–4 K near the tropical tropopause (Hack et al. 1998). In the cold pool an indication of an inversion appears at about 750 hPa in the model temperature profile that is not found in the ECMWF or NCEP reanalysis. ECMWF and NCEP are long-term climatological means for September and the model is only averaged over 30 days so it is understandable that any inversions in the reanalysis climatology have been smoothed. Soundings over the eastern Pacific Ocean show an inversion at about 800 hPa approximately half of the time (Yin and Albrecht 2000).

Cross sections of relative humidity with respect to

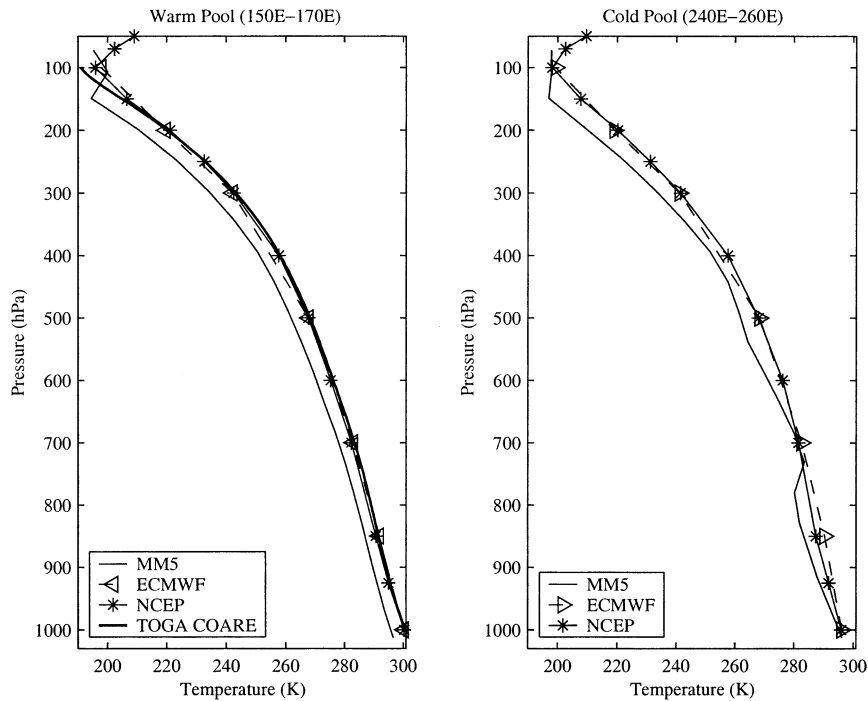


FIG. 2. Temperature profiles for the warm and cold pools. The warm pool profiles are averaged from 5°N to 5°S and from 150° to 170°E. The cold pool profiles are averaged from 5°N to 5°S and 240° to 260°E. The model is denoted with a thin solid line. The ECMWF reanalysis is denoted with triangles and a dashed line and the NCEP reanalysis is denoted with asterisks and a solid line. For the warm pool, a thick line denotes an average profile from TOGA COARE.

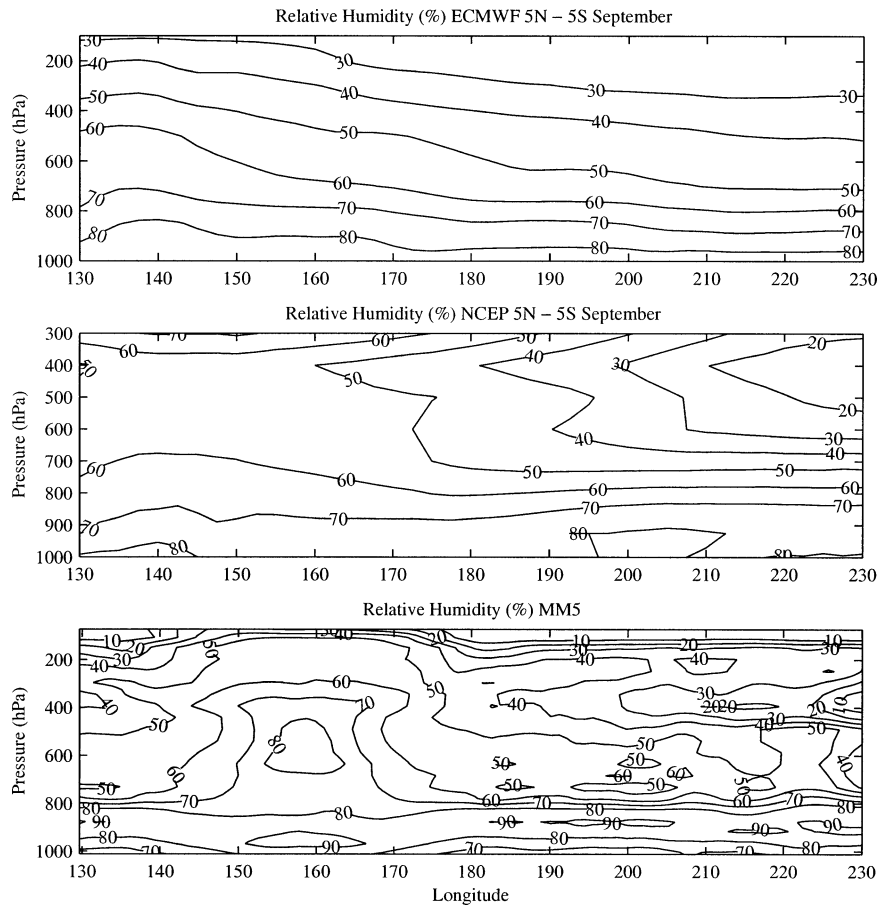


FIG. 3. Relative humidity cross section vs longitude for ECMWF and NCEP reanalysis and model data. The cross section is averaged from 5°N to 5°S. The reanalysis is for the Sep long-term mean.

water are shown for ECMWF and NCEP reanalysis September climatologies averaged from 5°N to 5°S and the model simulation (Fig. 3). NCEP shows a larger variation in upper-tropospheric relative humidities than ECMWF, which emphasizes that reanalysis from different weather prediction models are not consistent, especially for simulating the difference between convective and subsidence areas. Relative humidities above 80% cover more area in the model than the reanalysis. The maximum upper-tropospheric relative humidities occur at different longitudes: 137°E for ECMWF, 147°E for NCEP, and 160°E for the model. The maximum upper-tropospheric relative humidity in the model occurs above the maximum SST. The sinusoidal gradient of the model contributes to stronger convergence over the maximum SSTs than elsewhere. The reanalysis maximum of relative humidity may be influenced by the proximity of the maritime continent and warmer SSTs to the west of the warm pool than to the east.

The patterns of rising and sinking motion for the model and reanalysis data are shown in Fig. 4. NCEP reanalysis has stronger vertical motions than ECMWF. The vertical velocity field is very sensitive to model

details in the Tropics, and its value is not constrained very well by observations. The fraction of the area covered by the upward and downward motion is similar for all three datasets. The upper troposphere features descending motion and upward vertical motion extends less high as the SST decreases in every case. The vertical velocities are strongest in the model, because the longitudinal SST gradient is the only forcing of the atmosphere and it is constant for the entire simulation.

The cross section of zonal mass flux highlights the most visible difference between the model and the reanalysis (Fig. 5). In the model there is an upper-tropospheric heating over the warmest SST, and the resulting circulation in the upper troposphere causes a large zonal mass flux confined to the upper troposphere. The upper-tropospheric heating is also associated with high relative humidity, large vertical velocity, and large high cloud amount. The zonal mass fluxes for NCEP and ECMWF differ in magnitude and vertical structure.

The cloud properties of the model are compared with the International Satellite Cloud Climatology Project (ISCCP). The ISCCP dataset has a $2.5^\circ \times 2.5^\circ$ grid and data values of cloud percentages, categorized by cloud-

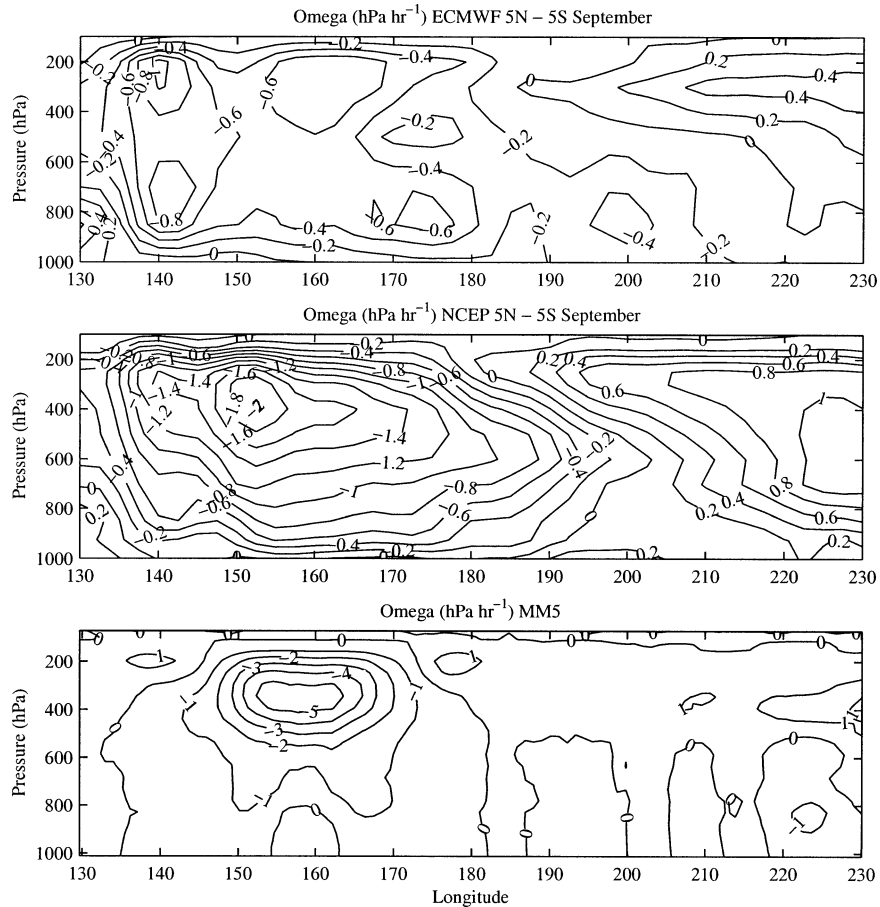


FIG. 4. Vertical pressure velocity cross section vs longitude for ECMWF and NCEP reanalysis and model data. The cross section is averaged from 5°N to 5°S. The reanalysis is for the Sep long-term mean. The values for the MM5 have been smoothed in the longitude direction so the zero contour is clearer.

top height and optical depth (Schiffer and Rossow 1985; Rossow and Schiffer 1999). In the model, radiation variables were stored every 30 minutes. The cloud top was defined to be the pressure where the visible optical depth of the cloud reached 0.1. The amount of cloud cover for each longitude averaged from 5°N to 5°S is shown for ISCCP and the model (Fig. 6). High clouds are defined to have cloud tops above 440 hPa, and low clouds are defined to have cloud tops below 680 hPa and the total cloud cover is also shown. ISCCP data show middle level clouds, but their percentage is about 10% across the entire domain. The percentage of middle clouds in the model is less than 1%. The most cloud cover is in the west due to the SST maxima, and the least is in the east. The model has a region of greater than 80% high cloud coverage over the warmest SSTs that is not seen in ISCCP. The low cloud amounts for ISCCP and the model are almost identical, and vary similarly with longitude. In summary, the model has a local maximum of high clouds that is not found in ISCCP, but the low cloud amounts agree very well.

The top of the atmosphere (TOA) radiation fluxes in

the model are compared to observations from the Earth Radiation Budget Experiment (ERBE) dataset, which are based on satellite measurements over the oceans. In Fig. 7, the clear-sky OLR and average-sky OLR are shown. The model OLR is much lower than ERBE observations between 152° and 162°. This discrepancy arises because the high clouds are concentrated above the warmest SST in the model. The clear-sky OLR has more variation for the ERBE data than for the model. Figure 8 shows the net absorbed solar radiation for clear skies and the all-sky average. The model has more variations than the ERBE data for the all-sky average. The model clear-sky absorbed shortwave is higher and more uniform than the ERBE data, possibly due to the lack of aerosols in the model. The average ERBE and model values are similar in the east. The region with the model cloud cover maximum has low absorbed shortwave values. The main difference between the model and the cloud and radiation data is that the convective cloud is concentrated over the warmest water in the model and not so in the observations. This discrepancy may be due to the greater large-scale variability in the real atmo-

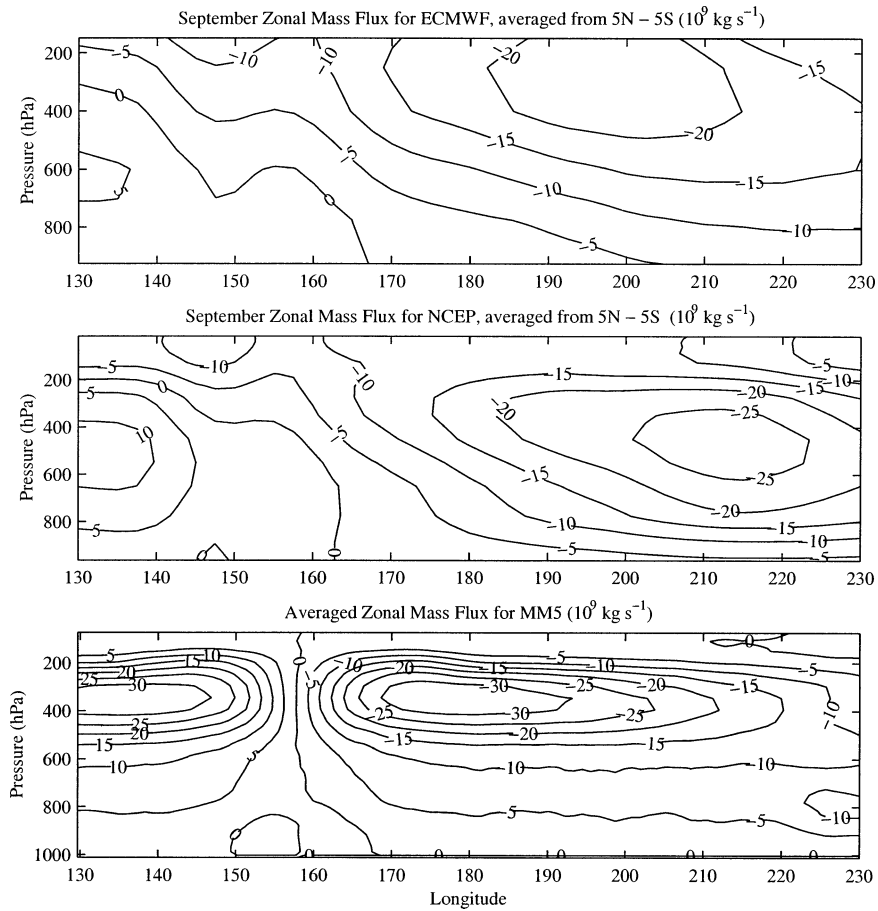


FIG. 5. Zonal mass flux cross section vs longitude for ECMWF and NCEP reanalysis and model data. The cross section is averaged from 5°N to 5°S. The reanalysis is for the Sep long-term mean.

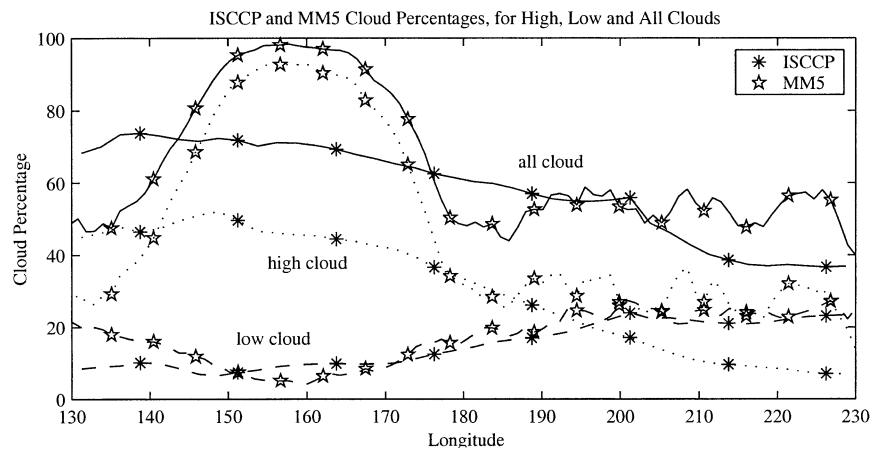


FIG. 6. Percentage of clouds vs longitude for ISCCP and model data. The total cloud amount (solid), high cloud amount (dotted), and low cloud amount (dashed) are shown. The annual average is denoted by asterisks and the model by stars.

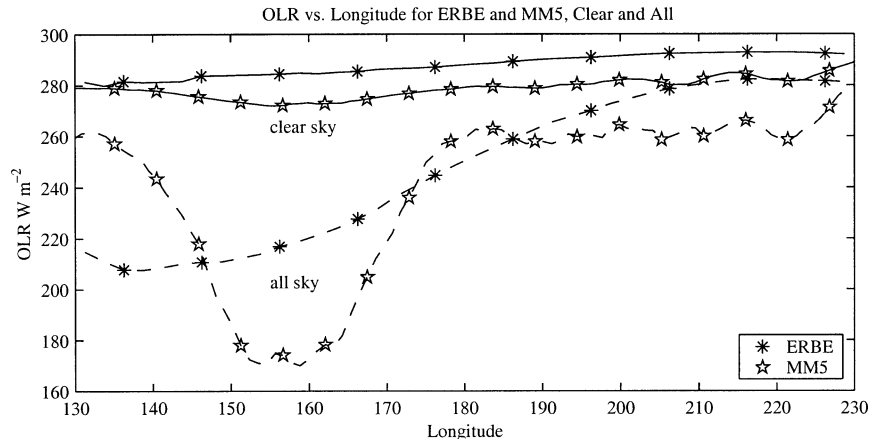


FIG. 7. OLR vs longitude for ERBE and model data. The clear-sky (solid) and all-sky (dashed) values are shown. The annual average is denoted by asterisks and the model by stars.

sphere compared to the model. Considering the simplification of the model, the agreement in the values and longitudinal gradients between the model and reanalysis is generally good.

3. Large-scale circulation, maximum SST, and SST gradients

The results of several sinusoidal SST gradient simulations with varying ranges and means provide insights about the role of large-scale circulation. Figure 9 shows the SST distribution for five experiments. The experiments are named for the mean SST and for the range of SSTs in the distribution. Simulation M300R4 has a mean of 300 K and a range of 4 K. Figure 10 shows the cloud water variables for simulations with a mean of 300 K and increasing SST ranges of 4, 6, and 8 K. A transition from low and liquid water stratus clouds in the subsidence region over the coldest SST to high thick ice clouds over the warmest SSTs is evident. The

width of the cloud ice 0.001 g kg^{-1} contour narrows as the SST range increases and the extent of the liquid cloud water increases, as shown by the 0.01 g kg^{-1} contour. Figure 11 shows the temperature tendencies due to dynamical heating (horizontal and vertical advection), moist convection and condensation (diabatic heating), and radiation for the M300R6 simulation. In Figs. 10 and 11 vertical lines have been drawn to identify regions of subsidence and low clouds, shallow convection, convection, and intense deep convection. The boundaries are used to describe regions with different balances between radiation, dynamics, and moist convection and condensation, as explained in the next paragraphs.

The intense deep convection region, A, is over the warmest SSTs. This region has high humidity, over 70% high cloud cover, a temperature profile that follows a moist adiabat, and upward motion that peaks at about 2 cm s^{-1} near 300 hPa. The net radiative heating rate is small and positive in the upper troposphere and at the ground. The moist convection and condensation

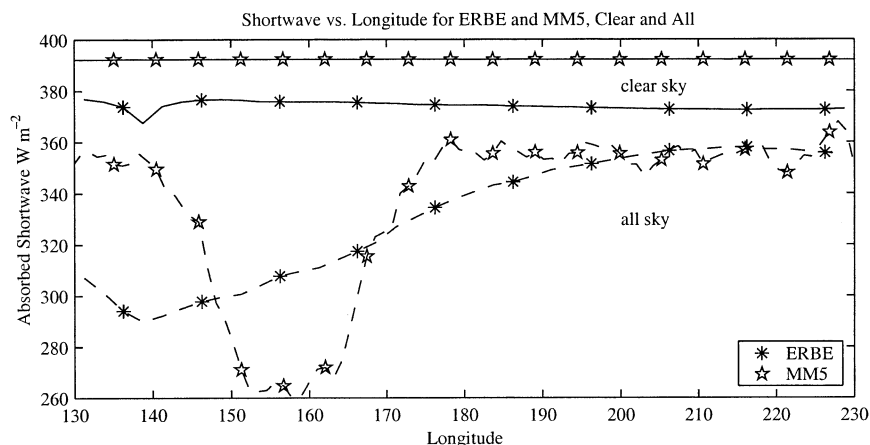


FIG. 8. The net absorbed solar radiation vs longitude for ERBE and model data. The clear-sky (solid) and all-sky (dashed) values are shown. The annual average is denoted by asterisks and the model by stars.

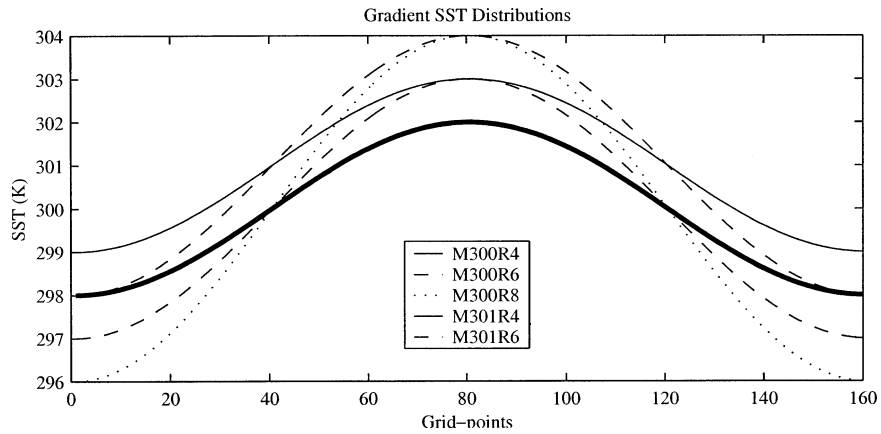


FIG. 9. SST distributions for five different simulations. M300R4 stands for a mean SST of 300 K and a SST range of 4 K, and other abbreviations also show the mean and range of the SST distribution.

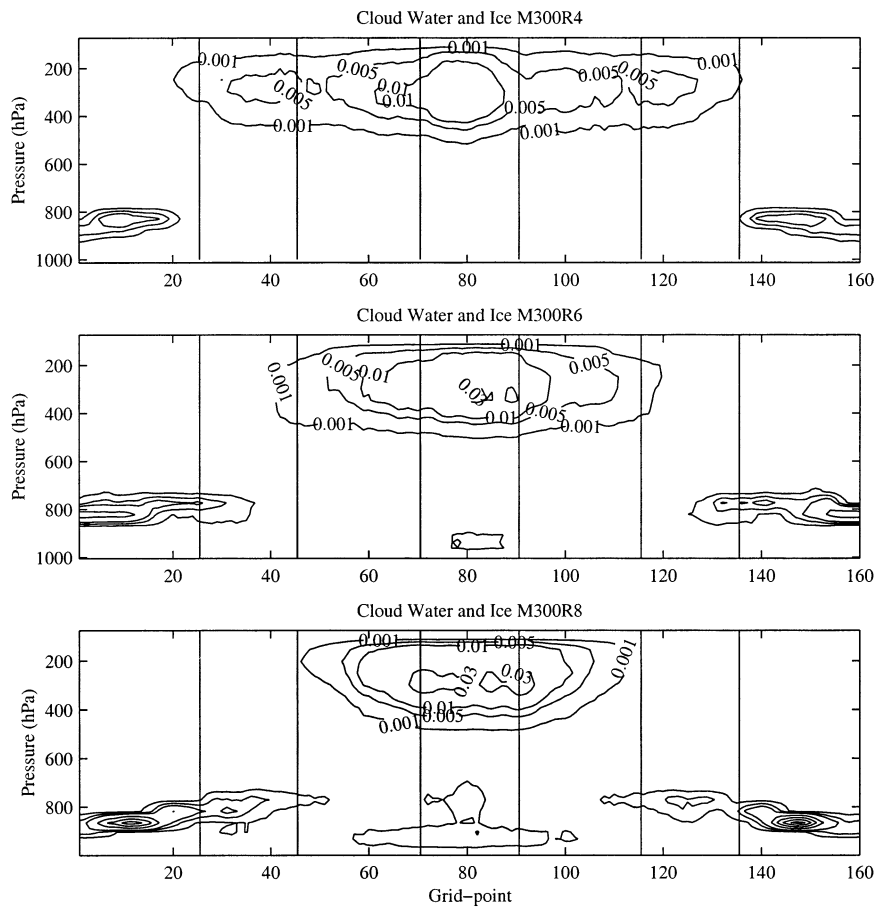


FIG. 10. Cloud liquid water (low altitudes), and cloud ice (high altitudes) for simulations M300R4, M300R6, and M300R8. The contours of cloud liquid water are 0.01 g kg^{-1} , 0.03 g kg^{-1} , 0.05 g kg^{-1} , and every 0.05 g kg^{-1} after that. The contours of cloud ice are labeled in g kg^{-1} and are 0.001 , 0.005 , 0.01 , and 0.02 intervals until the maximum.

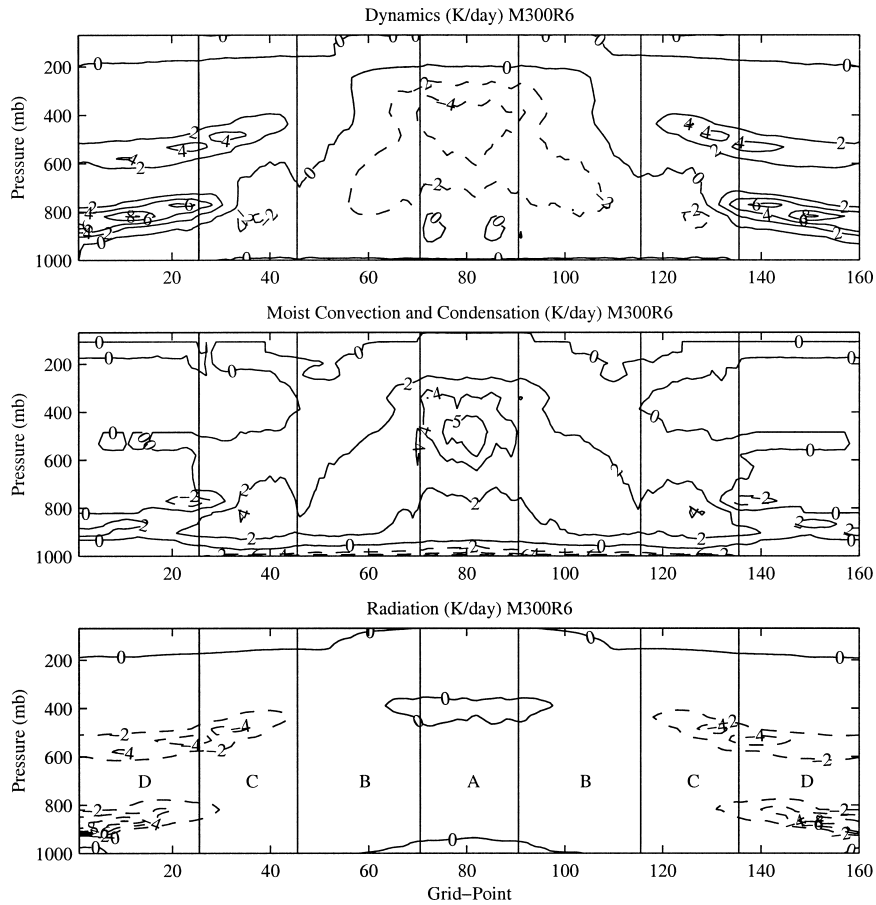


FIG. 11. The temperature tendency for the dynamics, moist convection and condensation, and radiation in K day^{-1} for the experiment with a mean SST of 300 K and a range of 6 K. Negative contours are dashed and positive contours are solid. The contour interval is 2 K day^{-1} . The average for the days 60–90 of the experiments shown. The letters A, B, C, and D represent different regions of the simulation as explained in the text.

peaks at about 400 hPa and is balanced by dynamical cooling forced by rising motion.

The convection region, B, is next to the intense deep convection region. The moist convection and condensation peaks in this region at about 700 hPa and is balanced approximately equally by dynamical cooling and radiative cooling. The temperature profile follows a moist adiabat and the relative humidity is over 50%. The vertical velocity is smaller than in the intense convection region and peaked lower in the atmosphere; it is negative above 250 hPa and positive below that level, never exceeding 0.5 cm s^{-1} . The high cloud covers about half of the region and low clouds cover about 20% of the region.

The shallow convection region, C, is adjacent to the convection region and over SSTs that are on average colder than the mean temperature of the experiment. The temperature profile features a stable layer, which is the trade inversion. The relative humidity is lower above the trade inversion. The vertical velocity is slightly positive near the surface and negative (about 0.5 cm s^{-1})

in the upper troposphere. The level of the zero vertical velocity changes with the SST gradient, and where the velocity is negative, radiative cooling balances subsidence warming. The low cloud amount is about 30% in this region and the high cloud amount decreases as the subsidence increases in this region. Recently, Johnson et al. (1999) have emphasized the role of midlevel convection, cumulus congestus clouds that detrain at the freezing level. The shallow convection (C) and convection (B) regions contain the midlevel convection in these simulations.

The subsidence region, D, is over the coldest SSTs in the experiment. In this region radiative cooling balances subsidence warming. The vertical velocity is negative everywhere below the top three levels of the model. The upper-tropospheric relative humidity is only about 15%. The temperature profile has stable layers at the height of the trade inversion and above the freezing level.

Figure 12 shows the zonal mass flux, rising motion in the center of the domain over the warmest SST and

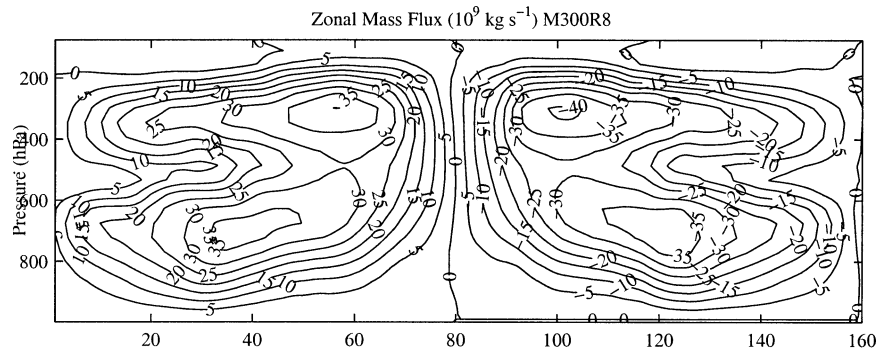


FIG. 12. Zonal mass flux averaged over latitude for 30 days for the simulation with a mean SST of 300 K and an SST range of 8 K.

sinking motion over the coldest SSTs for simulation M300R8. The closed circulation in the upper troposphere is also visible in Fig. 5 but there is an additional closed circulation in the lower troposphere near the coldest SSTs. The lower-tropospheric circulation becomes more pronounced in the simulations with greater SST ranges and creates a double-celled circulation. Interestingly, Grabowski et al. (2000) also found a double circulation in their CRM simulation forced by a sinusoidal temperature gradient. Their double circulation was attributed to the deviation of their quasi-equilibrium temperature profile from an observed tropical temperature sounding. The temperature profile is established by the radiative heating profile, which features a smaller cooling in the upper troposphere than is found in tropical observations when the radiation interacts with the clouds in the CRM. The radiative cooling profile in these simulations is also smaller than observed in the tropical upper troposphere, contributing to the double-celled circulation. Yano et al. (2002a,b) perform further analysis of the CRM SST gradient simulations, showing the deep mode of the Walker circulation is unstable in their simulations and simple dynamical balances. Above the trade inversion, the vertical velocity given by the balance between radiative cooling and subsidence warming matches the vertical velocities in these simulations, as is shown in Yano et al. (2002a) for CRM simulations and NCEP reanalysis of the Walker Circulation.

The upper circulation is a response to the heating by deep convection, which is strongest between 300 and 500 hPa in the intense deep convection region. The

strength of the heating monotonically increases with the warmest SST. Part one of this study found convective heating in the upper troposphere increased with increasing uniform SST. A similar relationship is found between the maximum SST and the convective heating in the SST gradient simulations. The moist convection and condensation vertical profile in the intense convection region is similar to the profile deduced by Houze (1982) for mature tropical cloud clusters (Fig. 11). This profile, with the peak in the upper troposphere, produced a reasonable Walker Circulation in a linear steady-state model (Hartmann et al. 1984). The maximum SST and the maximum zonal mass flux above the freezing level are linearly related, as shown by five representative experiments in Table 1. For every degree increase in the maximum SST the upper-tropospheric zonal mass flux maximum increases 25% of its value for M300R6. The strength of the SST gradient has little effect on the upper zonal mass flux maximum.

In the subsidence region of Fig. 11 at about 850 hPa, negative values of radiative cooling are balanced by subsidence warming, shown by the dynamic temperature tendency. The region of radiative cooling is related to longwave cooling at the top of the stratus clouds and it is this longwave cooling that drives the lower circulation. Nigam (1997) found that lower-tropospheric longwave radiative cooling from stratocumulus cloud tops produces a strong dynamical forcing that can be inferred from reanalysis. A maximum of 3–4 K day⁻¹ for the radiative cooling is inferred over the east Pacific, which is comparable to values in the M300R4 experiment. The stratus longwave cooling creates a feedback that produces a rapid development of the coastal southerly surface-wind tendency and stratocumulus clouds from March to May along the equatorial South American coast (Nigam 1997). The maximum of radiative cooling at the top of the stratus clouds produces divergence in the boundary layer.

As the range of the SST distribution increases, the potential temperature difference between the moist-adiabatic value in the free troposphere (determined by the maximum SST) and the boundary layer value over the

TABLE 1. The maximum zonal mass flux values in the upper and lower troposphere for five experiments with sinusoidal SST gradients.

Name	Maximum SST (K)	Upper maximum (10^{12} g s^{-1})	Lower maximum (10^{12} g s^{-1})
M300R4	302	22.3	23.5
M300R6	303	32.4	33.1
M300R8	304	40.4	38.3
M301R4	303	29.3	15.6
M301R6	304	35.6	30.6

TABLE 2. The rain rate, high and low cloud cover amounts, and integrated water variables for five experiments with sinusoidal SST gradients.

Name	Average rain rate (mm day ⁻¹)	Integrated ice (10 ³ g kg ⁻¹)	Integrated water vapor (kg m ⁻²)	High cloud cover (%)	Low cloud cover (%)	Integrated liquid water (10 ³ g kg ⁻¹)
M300R4	3.21	12.7	35.6	36.3	27.3	14.2
M300R6	3.71	14.2	38.5	31.3	27.5	27.3
M300R8	3.87	15.9	40.6	32.2	33.4	39.2
M301R4	3.24	14.4	37.9	35.7	22.1	8.9
M301R6	3.79	16.3	42.2	35.4	26.7	24.0

coldest SSTs increases. Klein and Hartmann (1993) found a strong positive correlation between the lower-tropospheric stability and cloud area fraction in stratocumulus regions. Thus, increasing the SST range increases the low cloud amount, and increases the amount of radiative cooling at the top of the stratus clouds. The radiative cooling increase forces an increase in the lower-tropospheric zonal mass flux. The lower-tropospheric zonal mass flux increases about 12% of its value in M300R6 for every degree increase in the SST range. When the mean temperature is increased with the SST range fixed at 6 K, the lower zonal mass flux maximum decreases at a rate of $-14\% \text{ K}^{-1}$. The lower zonal mass flux maximum decreases because the low cloud amount and associated radiative cooling decrease. The low cloud amount is found to decrease with increasing SST in observations (Klein and Hartmann 1993; Norris and Leovy 1994).

Another region of large radiative cooling and subsidence warming values occurs at about 550 hPa in the subsidence region. A steep gradient in specific humidity produces the large radiative cooling at that level, the temperature profile has a stable layer at that level as well. The lower circulation causes the moisture gradient. Air descending in the upper troposphere rose in the deep convection over the warmest SST and has descended from about 200 mb, decreasing the relative humidity of the parcel. Some air in the lower circulation ascends over the mean SST of the SST distribution and is much more humid because the parcel moves laterally from convection at a much lower altitude in the troposphere. The strong gradient occurs where the dry air from above meets the moister air in the shallow circulation.

Cloud-top longwave cooling is a positive feedback on the lower large-scale circulation. Greater longwave radiative cooling forced by the stratus clouds would cause a stronger lower-tropospheric circulation. Stronger radiative cooling creates more stratus clouds, which further strengthens the radiative cooling and would be balanced by a stronger large-scale circulation. A stronger lower-tropospheric circulation may advect more humidity over the stratus making the air moister in the lower half of the troposphere. The increased moisture will reduce the longwave radiative cooling produced by the stratus clouds. Moisture advection by the shallow

circulation may thus act as a negative feedback on the lower-tropospheric circulation.

A simulation in which the radiative effect of the low cloud was omitted was performed to test how much the radiative cooling from the low clouds contributed to the strength of the large-scale circulation. The lower-tropospheric circulation in experiment M300R4 was reduced 13% by eliminating the radiative cooling of low clouds. A stronger humidity gradient developed at the top of the boundary layer that enhanced the clear-sky radiative cooling, partly compensating for the missing radiative cooling by the boundary layer clouds. The height of the boundary layer and the height of the moisture gradient in the upper troposphere were both decreased in the simulation with radiatively inactive warm clouds.

4. Rain, clouds, and integrated water values

In these simulations with sinusoidal SST gradients, the largest amounts of rain occur over the warmest SSTs, and the smallest amounts occur over the coldest SSTs. The average precipitation rate for five different experiments is given in Table 2. The mean rain rate increases 0.18 mm day^{-1} for a 1° increase in the SST range. The rain rate increases 0.06 mm day^{-1} for each degree of mean temperature increase. The rain rate increases are associated with increases in the large-scale circulation strength. As the SST range increases, the lower and upper circulations increase in strength, while only the upper circulation increases as the mean SST is increased. The rain rate increase is larger for the SST range increase, since both circulations increase with SST range. In CRM experiments with a fixed cold pool temperature and increasing warm pool SST, SLLC also found the average rain rate increased because of the increasing strength of the large-scale circulation.

The average value of integrated cloud ice is proportional to the maximum SST (Table 2). In part one of this study the integrated cloud ice amount was found to increase with SST for uniform SST simulations. The concurrent increases in maximum SST and integrated cloud ice are consistent with part one since the deepest convection in the domain occurs over the maximum SSTs.

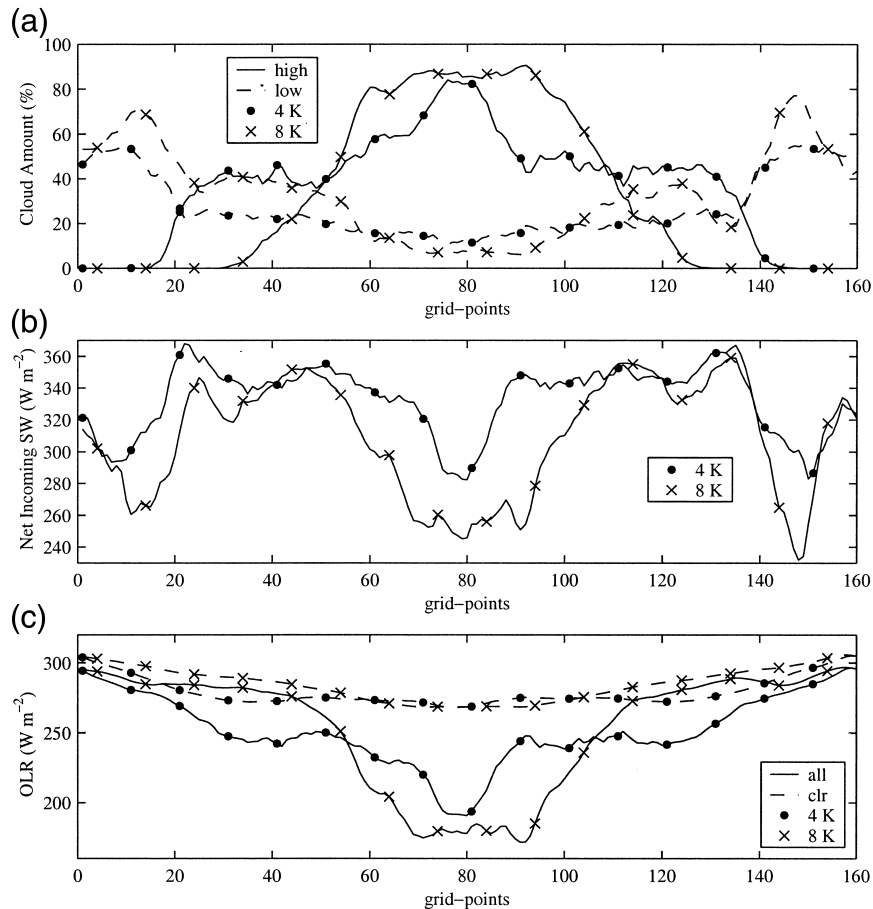


FIG. 13. (a) The high cloud amount and low cloud amount, (b) net incoming shortwave radiation (SWI), and (c) average OLR and clear-sky OLR for each longitudinal grid point for days 60–90 of the experiment. The numerical experiments with a mean SST of 300 K and a sinusoidal SST gradient of 4 K (circles) and 8 K (crosses) are shown.

The average value of integrated water vapor is also related to the maximum SST (Table 2). The average relative humidity is similar for these cases so the integrated water vapor amount is related to the mean temperature. The temperature for most of the troposphere is determined by the moist adiabat in the region with the maximum SST, causing the integrated water vapor amount to be related to the maximum SST. The percentage of high cloud cover is nearly constant at 35% in all the simulations.

The low cloud cover and the integrated liquid water are very related quantities since the low clouds are made of liquid water (Table 2). Liquid water is also found at low levels in high clouds. Both quantities vary similarly to the strength of the lower-tropospheric large-scale circulation. Since the lower-tropospheric large-scale circulation is driven by the radiative cooling at the top of stratus clouds, we would expect the circulation strength and low cloud amount to vary in similar ways. The low cloud amount decreases approximately $4\% \text{ K}^{-1}$ as the minimum SST of the simulation increases. The annual stratus cloud amount was found to decrease about

$5\% \text{ K}^{-1}$ in the region between 10°N and 10°S and 80° – 100°W in the eastern Pacific (Klein and Hartmann 1993). Since the low clouds in these simulations are found over the minimum SSTs and the minimum tropical Pacific SSTs are found in the region mentioned above, the agreement in changes of low cloud amount is excellent.

Figure 13a shows the cloud fraction for each longitude for simulations M300R4 and M300R8. The area of the domain covered by at least 20% high clouds decreases, while the area covered by at least 70% high clouds increases as the SST range increases. In other words, the increase of the large-scale circulation acts to concentrate the high clouds in a smaller fraction of the domain. Other studies (Bretherton and Sobel 2002; SLLC) also find that the convective fraction of the domain decreases with increased SST gradient.

5. Radiation

In this section we describe the sensitivity of the radiation budget at the top of the atmosphere to mean SST

TABLE 3. Radiation quantities at the TOA averaged over latitude and for days 60–90 for five experiments with sinusoidal SST gradients. The quantities are SWI, shortwave cloud forcing, (SW CF), OLR, clear-sky OLR, longwave cloud forcing, (LW CF), the blackbody emission for the given SST distribution (σT^4) and the clear-sky greenhouse forcing ($\sigma G_{\text{clr}} = T^4 - \text{OLR}_{\text{clr}}$).

Name	SWI (W m^{-2})	SW CF (W m^{-2})	OLR (W m^{-2})	OLR clear-sky	LW CF (W m^{-2})	σT^4 (W m^{-2})	G_{clr} (W m^{-2})
M300R4	332.7	−59.4	251.3	279.1	27.8	459.3	180.3
M300R6	324.7	−67.6	256.7	283.3	26.6	459.4	176.1
M300R8	308.4	−84.0	254.0	285.0	31.0	459.5	174.6
M301R4	341.5	−50.8	253.3	281.4	28.1	465.5	184.1
M301R6	324.0	−68.5	255.3	286.0	30.7	465.6	179.5

and SST range. Changing the SST gradient and mean SST does not strongly affect the average outgoing longwave radiation, but a degree increase in the SST gradient decreases the net absorbed shortwave radiation (SWI) approximately -5.6 W m^{-2} (Table 3). The average optical depth of clouds increases with SST gradient and, generally, the total cloud amount also increases with increasing SST gradient. The decrease in SWI is associated with an increase in the lower-tropospheric large-scale circulation. An increase in the large-scale circulation corresponds to stronger rising motion over the warmest SST, which creates more cloud water. A 25% increase in the lower maximum zonal mass flux of M300R4 leads to a 7.4 W m^{-2} decrease in the SWI. Figure 13b shows SWI for the M300R4 and M300R8 simulations. M300R8, with a larger lower-tropospheric large-scale circulation, has less SWI over the warmest SSTs and in the regions with more low clouds. The decreases in SWI are due to increased cloud liquid water in the stratus regions and at lower levels in the high clouds.

The domain-averaged OLR is very similar for all the experiments. The cloud-top temperature where the visible optical depth reaches 0.1 is approximately constant in all the simulations (Hartmann and Larson 2002). Figure 13c shows the OLR distribution for experiments M300R4 and M300R8. The average OLR is 2.7 W m^{-2} higher in simulation M300R8. The average clear-sky OLR is 5.9 W m^{-2} higher in simulation M300R8, which has the greater maximum SST. The temperature profile in the gradient experiments above the boundary layer is similar to the moist-adiabatic profile in the intense deep convection region over the warmest SSTs, causing the clear-sky OLR to increase as the maximum SST increases. The clear-sky greenhouse effect is defined as blackbody radiation at the SST minus clear-sky OLR, and it decreases with increasing SST gradient. Changes in the SST gradient do not strongly affect the average surface blackbody emission, but the clear-sky OLR increases with SST gradient because the maximum SST increases the air temperature everywhere and the domain-averaged upper-tropospheric relative humidity slightly decreases with increasing SST gradient (Table 3).

The clear-sky greenhouse effect is greatest in regions of high upper-tropospheric humidity, which have been

shown to occur near deep convection (Udelhofen and Hartmann 1995; Salathe and Hartmann 1997). If the SST gradient is held constant and the mean SST is increased, the longwave cloud forcing increases about $2 \text{ W m}^{-2} \text{ K}^{-1}$ and the clear-sky greenhouse effect increases about $3.5 \text{ W m}^{-2} \text{ K}^{-1}$. The sum of these two positive feedbacks approximately cancel the longwave emission increase associated with the imposed temperature increase.

6. Conclusions

This research demonstrates the important effects of the SST gradients and large-scale circulation on tropical climate sensitivities. Simulations with imposed fixed SST gradients are similar to averaged observations over the Pacific, when the discrepancies of large-scale dynamical forcing and constant full period sinusoidal SST gradients are taken into account. The simulations with sinusoidal SST gradient give distinct upper and lower zonal mean circulations in the troposphere. The upper circulation is sensitive to the heating from deep convection over the warmest SST and the lower circulation is sensitive to radiative cooling produced by stratus clouds.

Increasing the mean SST decreases the strength of the lower-tropospheric large-scale circulation. In a coupled GCM with doubled carbon dioxide, Knutson and Manabe (1995) found an increase in Pacific SST. In the warm pool region they found precipitation enhanced by 15%, but a decrease in the strength of the ascending vertical motion. Those results were explained as a consequence of the moist-adiabatic lapse rate decrease with increasing SST, which is also consistent with these fixed SST gradient experiments.

The absorbed shortwave radiation is found to be extremely sensitive to the SST gradient. The stronger lower-tropospheric large-scale circulation produces a higher water content in the high and low clouds, increasing the absolute magnitude of the shortwave cloud forcing. The shortwave effect is larger than the small changes in the OLR, and leads to a decrease in net TOA radiation with increasing SST gradient.

Increasing the mean SST creates a positive feedback in these simulations because of the decrease in the lower-tropospheric large-scale circulation and the simulta-

neous decrease in cloud optical depth. As the mean SST increases, low clouds cover a smaller area in the smaller subsidence region, so that the net negative cloud forcing of the low clouds is reduced, producing a net positive feedback. The increased SST decreases the high cloud OLR value and increases the water vapor amount, both of which are positive feedbacks. These effects are offset by the increase in longwave emission with increasing temperatures, but the positive feedbacks are larger. The effects are stronger for the simulations with a range of 4 K than the simulations with a range of 6 K.

The atmospheric large-scale circulation is coupled to the organization of tropical convection, clouds, rain, and relative humidity. The reorganization of those quantities can have strong feedbacks on the tropical climate. Increasing the mean SST decreases the strength of the lower large-scale circulation, while increasing the spatial gradients of SST produces increases in the large-scale circulation. The large-scale circulation causes the greatest change in the net absorbed shortwave radiation, a 25% increase in the lower maximum zonal mass flux of M300R4 leads to a 7.4 W m^{-2} decrease in the net absorbed shortwave radiation. A 0.6-K increase in the SST gradient may be able to offset a 1° increase in the mean SST. The response of SST gradients and the accompanying changes in large-scale circulation can be responsible for significant climate feedbacks. The effect of the large-scale circulation on the cloud optical depth is very large according to these simulations and may play an important role in tropical climate sensitivities.

Our understanding of the tropical climate will benefit from applying the results of these simulations to observations. El Niño–Southern Oscillation (ENSO) produces periods where the east–west SST gradient across the Pacific is decreased and the Pacific mean SST is increased. Both SST tendencies we would associate with reduced shortwave cloud forcing. Comparing these results to cloud observations associated with ENSO can illuminate the robustness of increasing shortwave cloud forcing with increasing large-scale circulation.

Acknowledgments. This research was supported by NASA Grant NAGS5-10624. The help of Miriam Zuk, Jim McCaa, and Marc Michelsen was invaluable. The comments of two anonymous reviewers and Chris Bretherton improved the manuscript.

REFERENCES

- Betts, A. K., 1990: Greenhouse warming and the tropical water budget. *Bull. Amer. Meteor. Soc.*, **71**, 1464–1465.
- Bretherton, C. S., and A. H. Sobel, 2002: A simple model of a convectively-coupled Walker circulation using the weak temperature gradient approximation. *J. Climate*, **15**, 2907–2920.
- Cess, R. D., 1975: Global climate change: An investigation of atmospheric feedback mechanisms. *Tellus*, **27**, 193–198.
- Grabowski, W. W., J.-I. Yano, and M. W. Moncrieff, 2000: Cloud resolving modeling of tropical circulations driven by large-scale SST gradients. *J. Atmos. Sci.*, **57**, 2022–2039.
- Grenier, H., and C. S. Bretherton, 2001: A moist PBL parameterization for large-scale models and its application to subtropical cloud-topped marine boundary layers. *Mon. Wea. Rev.*, **129**, 357–377.
- Hack, J. J., J. T. Kiehl, and J. W. Hurrell, 1998: The hydrologic and thermodynamic characteristics of the NCAR CCM3. *J. Climate*, **11**, 1179–1206.
- Hartmann, D. L., and M. L. Michelsen, 1993: Large-scale effects on the regulation of tropical sea surface temperatures. *J. Climate*, **6**, 2049–2062.
- , and K. Larson, 2002: An important constraint on tropical cloud–climate feedback. *Geophys. Res. Lett.*, **29**, 1951, doi:10.1029/2002GL015835.
- , and M. L. Michelsen, 2002a: No evidence for iris. *Bull. Amer. Meteor. Soc.*, **83**, 249–254.
- , and —, 2002b: Reply. *Bull. Amer. Meteor. Soc.*, **83**, 1349–1352.
- , H. H. Hendon, and R. A. Houze Jr., 1984: Some implications of the mesoscale circulations in cloud clusters for large-scale dynamics and climate. *J. Atmos. Sci.*, **41**, 113–121.
- Houze, R. A., Jr., 1982: Cloud clusters and large-scale vertical motions in the Tropics. *J. Meteor. Soc. Japan*, **60**, 396–410.
- Johnson, R. H., T. M. Rickenbach, S. A. Rutledge, P. E. Ciesielski, and W. H. Schubert, 1999: Trimodal characteristics of tropical convection. *J. Climate*, **12**, 2397–2418.
- Klein, S. A., and D. L. Hartmann, 1993: The seasonal cycle of low stratiform clouds. *J. Climate*, **6**, 1587–1606.
- Knutson, T. R., and S. Manabe, 1995: Time-mean response over the tropical Pacific to increased CO_2 in a coupled ocean–atmosphere model. *J. Climate*, **8**, 2181–2199.
- Larson, K., and D. L. Hartmann, 2003: Interactions among cloud, water vapor, radiation, and large-scale circulation in the tropical climate. Part I: Sensitivity to uniform sea surface temperature changes. *J. Climate*, **16**, 1425–1440.
- , —, and S. A. Klein, 1999: The role of clouds, water vapor, circulation, and boundary layer structure in the sensitivity of the tropical climate. *J. Climate*, **12**, 2359–2374.
- Lau, K. M., C. H. Sui, M. D. Chou, and W. K. Tao, 1994: An inquiry in to the cirrus-cloud thermostat effect for tropical sea surface temperature. *Geophys. Res. Lett.*, **21**, 1157–1160.
- Lindzen, R. S., 1990a: Some coolness concerning global warming. *Bull. Amer. Meteor. Soc.*, **71**, 288–299.
- , 1990b: Response. *Bull. Amer. Meteor. Soc.*, **71**, 1465–1467.
- , M.-D. Chou, and A. Y. Hou, 2001: Does the earth have an adaptive infrared iris? *Bull. Amer. Meteor. Soc.*, **82**, 417–432.
- , —, and —, 2002: Comment on “No evidence for iris.” *Bull. Amer. Meteor. Soc.*, **83**, 1345–1349.
- Manabe, S., and R. T. Wetherald, 1967: Thermal equilibrium of the atmosphere with convective adjustment. *J. Atmos. Sci.*, **24**, 241–259.
- McCaa, J., 2001: A new parameterization of marine stratocumulus and shallow cumulus clouds for climate models. Ph.D. dissertation, University of Washington, 146 pp.
- Meehl, G., W. D. Collins, B. A. Boville, J. T. Kiehl, T. M. L. Wigley, and J. M. Arblaster, 2000: Response of the NCAR climate system model to increased CO_2 and the role of physical processes. *J. Climate*, **13**, 1879–1898.
- Miller, R. L., 1997: Tropical thermostats and low cloud cover. *J. Climate*, **10**, 409–440.
- Nigam, S., 1997: The annual warm to cold phase transition in the eastern equatorial Pacific: Diagnosis of the role of stratus cloud-top cooling. *J. Climate*, **10**, 2447–2467.
- Norris, J. R., and C. B. Leovy, 1994: Interannual variability in stratiform cloudiness and sea surface temperature. *J. Climate*, **7**, 1915–1925.
- Pierrehumbert, R. T., 1995: Thermostats, radiator fins, and the local runaway greenhouse. *J. Atmos. Sci.*, **52**, 1784–1806.
- Ramanathan, V., and W. Collins, 1991: Thermodynamic regulation

- of ocean warming by cirrus clouds deduced from the 1987 El Niño. *Nature*, **351**, 27–32.
- Rossow, W. B., and R. A. Schiffer, 1999: Advances in understanding clouds from ISCCP. *Bull. Amer. Meteor. Soc.*, **80**, 2261–2287.
- Salathe, E. P., and D. L. Hartmann, 1997: A trajectory analysis of tropical upper-tropospheric moisture and convection. *J. Climate*, **10**, 2533–2547.
- Schiffer, R. A., and W. B. Rossow, 1985: ISCCP global radiance data set: A new resource for climate research. *Bull. Amer. Meteor. Soc.*, **66**, 1498–1505.
- Su, H., S. S. Chen, and C. S. Bretherton, 1999: Three-dimensional week-long simulations of TOGA-COARE convective systems using the MM5 mesoscale model. *J. Atmos. Sci.*, **56**, 2326–2344.
- Tompkins, A. M., and G. C. Craig, 1999: Sensitivity of tropical convection to sea surface temperature in the absence of large-scale flow. *J. Climate*, **12**, 462–476.
- Udelhofen, P., and D. L. Hartmann, 1995: Influence of tropical convective cloud systems on the relative humidity in the upper troposphere. *J. Geophys. Res.*, **100**, 7423–7440.
- Yano, J.-I., W. W. Grabowski, and M. W. Moncrieff, 2002a: Mean-state convective circulations over large-scale tropical SST gradients. *J. Atmos. Sci.*, **59**, 1578–1592.
- , M. W. Moncrieff, and W. W. Grabowski, 2002b: Walker-type mean circulation and convectively coupled tropical waves as an interacting system. *J. Atmos. Sci.*, **59**, 1566–1577.
- Yin, B., and B. A. Albrecht, 2000: Spatial variability of atmospheric boundary layer structure over the eastern equatorial Pacific. *J. Climate*, **13**, 1574–1592.